RSC Advances

ROYAL SOCIETY OF CHEMISTRY

www.rsc.org/advances

ROCK-regulated synergistic effect of macropore/nanowire topography on cytoskeletal distribution and cell differentiation

Houhua Pan[1,2], Youtao Xie[1], Kai Li[1], Dandan Hu[1], Jun Zhao[1], Xuebin Zheng[1*], Tingting Tang[2**]

[1]Key Laboratory of Inorganic Coating Materials, Shanghai Institute of Ceramics, Chinese Academy of Sciences, 1295 Dingxi Road, Shanghai 200050, People's Republic of China

Email address: *xbzheng@mail.sic.ac.cn

[2]Shanghai Key Laboratory of Orthopaedic Implants, Department of Orthopaedics, Shanghai Ninth People's Hospital, Shanghai JiaoTong University School of Medicine, Shanghai 200011, People's Republic of China

Email address: **tingtingtang@hotmail.com

Abstract

Nanotopographical modification of implants has been proved to be a promising approach to inducing osteogenesis, which has also been utilized to promote biological property of plasma sprayed titanium coating possessing macropore. However, less attention has been paid to the detailed process of cell-surface interaction and its mechanism especially related to the macro/nano structure. In this study, focus has been put on the early MC3T3 cell adhesion behaviors on macro/nano structured surface and its correlation with cell differentiation. Nanowire titanium (NT) structure has been produced by hydrothermal method, and introduced onto traditional plasma sprayed titanium coating (TPS) to obtain the nano-structured plasma sprayed titanium coating (NTPS). Results showed that NT surface was beneficial for filopodia generation and cell spreading, while cells on TPS surface could adapt themselves to the rough macroporous topography but poor spreading could be observed. The

hierarchical NTPS surface was able to make a synergistic effect, with better cell spreading attributed to nano topography and multi-dimensional cytoskeleton distribution caused by macroporous structure. Accordingly, different levels of cytoskeleton tension, with moderate Rho-associated kinase (ROCK) activity on NT and TPS but higher expression on NTPS could be observed. Consequently, NTPS had better differentiation performance compared to NT and TPS surface. After ROCK was inhibited, the difference between all groups diminished. It can be concluded that the better performance of NTPS in triggering cell differentiation may attribute to its higher cytoskeleton tension than NT and TPS, which was obtained by the synergistic effect of macro/nano-topography on cell spreading and cytoskeletal distribution.

Key words: macro/nano, synergistic effect, cytoskeleton, ROCK

Introduction

Titanium and its alloys have been widely applied in the clinic, especially in the orthopaedics due to their excellent mechanical properties and biocompatibility[1, 2]. However, their poor bioactivity, especially the unsatisfactory performance to induce rapid osteogenesis and osseointegration, may lead to probable unstable combination, followed by high risk of surgery failure and patient morbidity[3]. And so, rapid osteogenesis and firm fixation of implants has always been a challenge and pursuing.

As we know, bone tissues are natural hierarchical structures composed of nano-, micro-, and macro-scale building blocks[4]. From the biomimetic viewpoint, various kinds of structured surfaces have been fabricated on the titanium in order to enhance the whole cell responses. Many research works have proved that the topographic cues and characteristics of implant surface play critical roles in cell behaviors including adhesion, proliferation, differentiation and eventual osseointegration[5-7]. Considerable

amounts of technologies have also been applied to fabricate specific topographies on commercial implant products and good clinical performance has been obtained[8-10]. Plasma sprayed titanium coating (TPS) is one of the modification technology commonly used and has been proved to be fruitful. This coating with large roughness and macroporous structures can effectively encourage the bone tissue in-growth and form a mechanical interlocking with host bone tissues[11, 12]. However, owing to the passive bioactivity of Ti, problems still exist when considering the poor early cell responses such as adhesion efficiency, formation of focal adhesion and cytoskeletal spreading, which will directly influence the following cell behavior and the final bone formation[12-15]. In recent years, the interactions between cells and nanotopographies are of increasing interests and found to be efficient in promoting early cell functions[16, 17]. On this basis, hierarchical surfaces containing different scales of structural features simultaneously are gradually believed to provide a more suitable surface topography for cell functions as it can better mimic the structure of the natural extracellular matrix[18-20]. Thus, there have also been some attempts to fabricate nano-structured plasma sprayed titanium coating (NTPS) to improve its early osseointegration[12, 15, 21, 22]. On the whole, all these reports pointed out that the hierarchical macro/nano surface has comprehensive promotion on cell behaviors when compared to the pure rough coating. However, most of these studies just have paid primary attention to the materials preparation methods and their excellent biological performance. It is still unclear that why the hierarchical surfaces behave better and few studies focus on the detailed mechanism of how the macrotopography of TPS cooperated with the nanotexture. Thus, it is necessary that further study be carried out about the detailed process and probable mechanism of cell-surface interaction in TPS-based structures.

Surface topographies are supposed to directly influence the cell morphology and cytoskeleton distribution, which have been considered to be closely related with the cell fate orientation and osteogenic tendency. Mcbeath et al. found that well spread stem cell undergoes osteogenesis, while the poorly spread one becomes adipocytes[23]. This was attributed to the cytoskeleton tension caused by morphology change and the following intracellular mechanotransduction, which have been considered to play a critical role in osteogenesis inducement[24]. Besides, Benjamin et al.[25] reported that nanotopography induced hMSC differentiation through cell mechanotransduction modulated by FAK. It indicates that nanotopography can bring about changes of focal adhesion which accompany with cytoskeleton distribution, intracellular tension and finally influence differentiation[26]. Furthermore, Rho-associated kinase (ROCK), being vital to the cytoskeleton reorganization, can directly regulate focal adhesion formation and cell spreading. It causes intracellular tension when activated, which has been proved to contribute to cell differentiation[27, 28]. Considering these, it provides an insight to the problem mentioned above by studying the status of cell morphology and cytoskeleton distribution and the concomitant intracellular tension on different designed surfaces and find the bridge between surface topography and cell differentiation.

In this study, biomimetic macro/nano-textured surface was produced on plasma sprayed titanium coating by hydrothermal treatment. Besides, solo nano-texture and TPS surface were also fabricated for comparison in order to achieve a better understanding. The MC3T3 cells were used for evaluation. The purpose of this study was to focus on how the hierarchical structures influence cell morphology and cytoskeleton distribution as well as the following cytoskeleton tension, and confirm their correlation with cell differentiation.

Experiments

2.1 Sample preparation

Pure Ti substrates (Φ10 mm×2mm and Φ34 mm×2mm) were provided by Shenyang Zhonghang Titanium Co.,Ltd. Samples polished by 1# - 7# polishing paper (PT) were used as control. For fabricating nano-structured titanium surface (NT), the plates were firstly acid-etched in the mixed solution of hydrofluoric acid and Nitric acid (V_{HF}: V_{HNO3}: V_{H2O}=1:3:6) to remove the oxide layer, and ultrasonically cleaned twice in ethanol and deionized water. Then the plates were treated by 2.5M NaOH in a Teflon-lined vessel at 150^{o}C for 15h. After washing gently with deionized water, samples were finally annealed at 480^{o}C for 2h to make anatase the eventual chemical composition. Besides, TPS surfaces were fabricated by vacuum plasma spraying (VPS, F4-VB, Sulzer Metco, Switzerland). After ultrasonic cleaning, the above-mentioned hydrothermal method was applied to TPS to gain the NTPS surfaces .

2.2 Surface characterization

Field-emission scanning electron microscopy (Hitachi S-4800, Japan) was used for observation of the surface morphology of the samples. Surface roughness was quantified by a Stylus Profiler (HOMMEL-ETAMIC T8000). The chemical composition of the surface was detected using a thin-film x-ray diffractometer (D/max 2500PC, Rigaku, Tokyo, Japan) .

2.3 Cell culture

Mouse osteoblastic cell line MC3T3-E1 was obtained from the Cell Bank of the Chinese Academy of Sciences (Shanghai, China). Cells were cultured in DMEM

(Invitrogen) supplemented with 10% FBS (Hyclone) and 1% penicillin/streptomycin and incubated in a humidified atmosphere of 5% CO_2 at 37 ^{o}C. The growth medium was changed every 2 days and cells were passaged when they reached 80% confluence.

For osteogenic differentiation, the normal culture medium was supplemented with 100 nM dexamethasone (Sigma Aldrich), 50 μM ascorbate acid (Sigma Aldrich) and 10 mM β-glycerophosphate sodium (Sigma Aldrich). The media was renewed every 2 days.

2.4 Cell morphology

Cells were seeded onto each specimen at a density of 3×10^4 cells/well in a 24-well. After 24h of incubation, the samples were washed twice with PBS, fixed in 2% glutaraldehyde overnight, and washed twice again. Then cells were dehydrated in a graded series of ethanol (30, 50, 70, 90, 100%) to prevent deformation of cytoskeleton, and dried in 37 ^{O}C overnight[29, 30]. Finally the morphology of cells were observed by the SEM.

2.5 Cell cytoskeleton immunofluorescence

The cytoskeleton of cells on samples were observed by confocal laser scanning microscopy (CLSM, Nikon). After 24 h of incubation the specimens were washed gently twice with PBS and then fixed with 4% paraformaldehyde for 15 min at room temperature ,washing twice, and permeabilized with 0.1% Triton X-100 for 10 min. After washing three times, samples were immersed in 1% BSA solution for 1h for sealing. After washed by twice, cells were treated with rhodamine phalloidin (Molecular Probes) for 40 min in dark. After rinsing for three times, the cell nuclei

were stained with 40, 60-diamidino-2-phenylindole (DAPI, Sigma) at a concentration of 5μg/ml for 5 min without light. After thorough washing with PBS, cells were observed under confocal microscopy.

2.6 western blotting

To evaluate the cytoskeleton tension on different surfaces, the activity of ROCK II, which regulates the cytoskeleton reorganization, was assayed by phosphorylation of MYPT1, one of ROCK's substrates. In detail, cells on the surface were washed by PBS and carefully collected by Tyrisin after 3 days. After centrifugation and thorough cleaning three times with PBS, cells were treated by Ripa lysis buffer (Beyotime) with 1% protease inhibitor. After protein concentration of all samples were qualified, necessary volumes were calculated and equal protein of lysates were loaded into acrylamide gels for electrophoresis, and transferred onto a PVDF membrane (Millipore). Membranes were blocked with blotto (5% nonfat milk powder in PBS plus 0.1% Tween 20) for 1 hour at room temperature and incubated with specific primary antibodies (CST) at 4 °C overnight. Membranes were washed three times with PBS plus 0.1% Tween 20 and incubated with secondary antibody conjugated with HRP (CST) and subsequently incubated in chemiluminescent reagents and detected (Thermo Scientific, Waltham, MA). For quantitative analysis, photoshop was used to obtain densitometric values from developed films. MYPT1 activity was determined as a ratio of phosphorylated MYPT1 to GAPDH for each group. Meanwhile, all of the values of other three groups were presented relative to the corresponding results of PT.

2.7 Alkaline phosphatase activity assay

Cells were seeded with density of 5×10^4 cells/well in 48-well plates. After 7 and 14 days of culture with osteogenic inducing medium, the specimens were washed three times with PBS, and then lysed in a 0.2% Triton X-100 solution through three standard freeze–thaw cycles. Then alkaline phosphatase (ALP) activity was measured using an ALP assay kit (JianCheng, Nanjing, China). The total protein concentration was measured using the Micro-BCA kit (Pierce, America). The ALP activity was finally normalized to the total intracellular protein.

2.8 Matrix mineralization

5×10^4 cells were seeded into each well in 48-well plates. After culturing for 14 and 21 days, cells were washed twice with PBS and then fixed with 4% paraformaldehyde for 15 min at room temperature. After washing twice, cells were stained with 0.1% Alizarin Red (Sigma) in Tris-HCl (pH 8.3) for 10 min at room temperature. Afterwards, specimens were washed with distilled water until no unbound stain appeared. Then the stain on the samples was dissolved in10% cetylpyridinum chloride in 10 mM sodium phosphate (pH 7) on the shaking table and the absorbance values were finally measured at 590 nm.

2.9 Osteocalcin secretion

The expression of osteocalcin was detected by a Elisa kit. Briefly, 5×10^4 cells were seeded on each specimen. When it reached 14 and 21 days, osteocalcin was collected according to the instruction of Elisa kit (Biolegend). Then the concentration of osteocalcin was measured whereas the total protein content was determined by Micro-BCA kit. The final osteocalcin content was normalized to the total protein concentration.

2.10 Quantitative real-time PCR

The osteogenesis-related gene expression was assayed by real-time quantitative polymerase chain reaction (RT-qPCR). Cells were seeded on the samples in a 6-well plate at an initial density of 3×10^5 cells/well. After incubation of 14 days, total RNA was isolated using trizol (Life Technology), and quantitative real-time PCR was performed using an ABI 7500 Real-Time PCR System (Applied Biosystems, USA) with a PCR kit (SYBR Premix EX Taq, TaKaRa). The relative expression of Runx2, type I collagen (COL I), and osteopontin (OPN) were evaluated and β-actin was used as the internal control for normalization. All of the Gene expression of other three groups were presented relative to the corresponding results of polished titanium. The sequences of the forward and reverse primers used in this study are shown in Tab. 1.

2.11 Rock inhibition

To access the effect of cytoskeleton tension on osteogenesis, the ROCK signaling was inhibited using a ROCK-specific inhibitor, Y-27632 (CST). Y-27632 was used at a final concentration of 10 μM and added into standard osteogenic inducing media. The media was changed every two days to ensure continuous activity of the inhibitors. After 14 days, osteogenic gene expression was also detected by real-time PCR as previously mentioned.

2.12 Statistical analysis

All experiments were conducted in triplicate and repeated three times, and all the data were expressed as the means ± standard deviation (SD). Statistical differences were determined by methods of *T-test*. Values of $p< 0.05$ were considered to be statistically significant.

Results

3.1 Surface characterization

The surface morphologies of the fabricated samples were characterized by SEM (Fig. 1). The polished titanium was used as control (Fig. 1A). After hydrothermal treatment, relatively rough surface with submicron-scale features could be observed in the low magnification picture of NT surface (Fig. 1B). At a higher magnification, an anisotropic nanowire-like texture appeared with the wire diameters between 20-50 nm. In Fig. 1C, it could be observed that the TPS surface was composed by molten and flattened particles, which on the whole presented an irregular rough macroporous morphology. However, the coating surface was relatively smooth at nano-scale. After hydrothermal treatment, hierarchical structure with similar nanowires were found for NTPS surface while no obvious changes could be seen in the original micro-scale texture (Fig. 1D).

The XRD results (Fig. 2) showed that both the NT and NTPS surface was composed of Ti and anatase phases, while the surface of PT and TPS was supposed to be pure Ti, thus the consistency of the chemical composition of the four different surfaces could be guaranteed. The roughness of the surface without micro-structure was around 1μm while TPS and NTPS both presented a 15μm-level roughness, and this indicated that the nanowire structure did not make much sense to the roughness values (Table. 2).

3.2 Cell morphology and cytoskeleton fluorescence staining

The MC3T3 cells displayed dramatically different shapes after 24-h incubation on different substrates with various topographies, as shown in Fig. 3. On PT surfaces, Most of the cells presented spindle or round morphology with less-spread body and

few filopodia (Fig. 3A). However, with the introduction of nanowire, cells were more spread and exhibited a polygonal morphology with a relatively larger size (Fig. 3B). Specially in the high magnification picture, filopodia could be clearly seen in abundance (Fig. 3D). For the TPS surface, cells showed an elongated body which adapted themselves to the complicated rough topography of coating. However, poor cell spreading all around with few filopodia could be seen (Fig. 3C). On the hierarchical NTPS surface , cells went along with the coating's topography and spread well all around simultaneously. Large amounts of filopodia could also be seen on the edge of skeleton, presenting a good interaction with the nanowire texture (Fig. 3E-H).

The cytoskeleton fluorescence staining (Fig. 4) of four groups were largely corresponding to the above SEM images. The morphology of the cells on PT were mostly round, while it spread remarkably with abundant filopodia by the introduction of nanowires. Elongation of cytoskeleton could be found on the TPS, with relatively smooth edge. For the NTPS, analogous characteristics with NT, such as well-developed cytoskeletal stretching and large amounts of filopodia, could be seen. On the whole, it could be concluded that the nanowire structure could enhance cell spreading and filopodia generation, and TPS surface provided rough porous topography but cells spread poorly on it, while the hierarchical NTPS surface was able to play a synergistic effect, with better cell spreading, more visible filopodia and multidimensional cytoskeleton distribution simultaneously.

3.3 ROCK activity assay

To examine whether the specific cell morphology and cytoskeleton distribution aforementioned were related with the cytoskeleton tension, the ROCK activity was detected by phosphorylation of MYPT1, one of ROCK's substrate. Results showed

that after seeded by 3 days, the ROCK activity of cells on NT and TPS was greater than that on PT, while cells on NTPS presented higher ROCK activity than NT and TPS. For semi-quantitative analysis of the band, a more than 200% increase was observed for the NT and TPS surface when compared to PT, with no obvious difference between them. ROCK activity on NTPS was about 6 times than PT, and nearly 2 times than NT and TPS as well (Fig. 5). On the whole, cells on the NTPS possessed higher cytoskeleton tension, which maybe a synergetic effects of NT and TPS. It was also in accord with the cell morphology and cytoskeleton distribution aforementioned.

3.4 alkaline phosphatase activity

Alkaline phosphatase (ALP) was one of the most important markers of the early stage of cell differentiation and osteogenesis. ALP activity after 7 and 14 days of culture had been measured and the results are exhibited in Fig. 6. No matter on the 7^{th} or 14^{th} day, the ALP activity showed no significant enhancement for NT and TPS in contrast to PT, but the NTPS surface achieved an enormous improvement in ALP expression, which was promoted to about 164% of PT, 165% of NT and 136% of TPS on the 7^{th} day, and 162%,154% and 144% on the 14^{th} day.

3.5 Extracellular matrix mineralization and osteocalcin secretion

Extracellular matrix mineralization measured by quantification of Alizarin Red staining is shown in Fig. 7. The NT and TPS surfaces both enhanced mineralization and NTPS surface had better performance, which was about 195% of PT, 156% of NT, and 139% of TPS on the 14^{th} day. And on the 21^{st} day, the value turned out to be 191%, 153% and 135% respectively. The osteocalcin secretion was also assayed by ELISA and showed in Fig. 8. The tendency is similar to the extracellular matrix

mineralization that maximum could be found on NTPS. It is obvious that osteogenesis could be promoted by NT and TPS surface, and the combination of the two led to a further advance.

3.6 Real-time PCR and ROCK inhibition

The osteogenic gene expressions, including Runx2, COLI and OPN after 14 days, were quantified by real-time PCR (as revealed in Fig. 9). NT and TPS facilitated all of them in different degrees, while much higher expressions on the NTPS surface could be observed. According to the preceding results, different increases in the ROCK substrate phospho-MYPT demonstrated different levels of ROCK activation on different surfaces, especially higher expression on NTPS surface which might relate to its better differentiation performance. In order to further confirm the relationship between cytoskeleton tension and differentiation, ROCK activation was inhibited with Y27632. Results (Fig. 9) showed that after Rock activation was inhibited, all the three osteogenic gene expression on the 14^{th} day underwent a slide for all four groups. The gaps between different samples diminished significantly. It was obvious that the cytoskeleton tension regulated by ROCK was closely related to the cell differentiation behaviors on four groups.

Discussion

In this study, the hybrid macropore/nanowire surface topography (NTPS) was produced on titanium coating using alkaline hydrothermal method. It was naturally considered that this biomimetic structure could further enhance the overall biological performance. Our results suggested that the NT and TPS structure did play different

roles in cytoskeleton distribution, and the combination of the two could lead to a synergistic effect, which brought in extra cytoskeleton tension and corresponding effect on cell differentiation.

Nanostructures have been believed to have significant effect on early cell response. In this study, when seeded on nanowire surface, cells were outstretched and exhibited a polygonal morphology with extended filopodia. As a contrast, spindle or round shape with poor spread morphology could be found on polished surface. It is widely accepted that nano-scale structures can contribute to cell spreading[31, 32]. Besides, it could be seen in the magnification picture that filopodia extended approximately along the direction of certain nanowires. It seemed that both nano-scale effect and nanowire topography cooperatively contributed to the spread of cytoskeleton. Nano-scale effect is prevalently attributed to large specific surface area, high surface energy and high hydrophilia, which will benefit the specific protein adsorption and integrin expression. Higher integrin expression and more binding with adsorbed protein lead to more rapid focal adhesion formation, decomposition and reconstruction, which leads to better cell spreading[22,33-35]. On the other hand, the nanowire topography itself can be a guidance of the orientation of integrin clustering and focal adhesion reassembling owing to its proper diameter[36-39]. With all these features combined, NT surface contributes well to cell spreading.

Plasma sprayed titanium coating which possesses macroporous rough surface has been believed to be beneficial for the long-term stability of implants. In our study, cells on the TPS surface showed an elongated body cling to the surface. Meanwhile, the cell extended along the rough up-and-down topography formed by melted particles. As a result, three-dimensional cytoskeletal spread could be obtained. These phenomenons were common on TPS surface as reported[21, 22]. It was believed that the

topography cues could be translated by the integrins and further regulated by focal adhesion so the cells could recognize the topography and adjust to the environment[40-42]. But it must be pointed out that although rough surface was provided, poor cell spreading accompanying with little filopodia could be observed, leading to poor adaptation to the native rough surface topography and inferior cytoskeleton development.

It was a perfect combination that cells on the hierarchical NTPS surface greatly utilized the features of both macropores and nanowires. Cells spread well all around while went along with the coating's rough topography. Filopodia could also be detected in abundance as well. It seemed that the macro/nano topography could provide multi-dimensional cytoskeleton deformation alongwith well-spread cytoskeleton in the same time. This firstly attributed to that the macroporous topography of TPS could be maintained after nanotexture was introduced[43]. And as previously mentioned, solo NT and TPS surface could exert their influence in their special ways, with nanowires contributing to cell spreading as well as macroporous surface providing the basic rough topography which was responsible for the main cytoskeletal deformation. With the combination of these two necessary parts, synergistic effect was obtained on the NTPS surface.

Cytoskeleton tension has been considered to accompany with cell spreading and cytoskeleton reorganization and is known to be regulated by myosin II, which is activated by phosphorylation of myosin light chains (MYL). MYL phosphorylation is regulated by the equilibrium between the activities of Ca^{2+}/calmodulin-dependent myosin light chain kinase (MLCK) and myosin light chain phosphatase (MLCP). MLCP is inhibited by phosphorylation of its myosin-targeting subunit (MYPT1), which is operated by Rho-associated kinase (ROCK). Through phosphorylation of

MYPT1, ROCK makes a effect on MYL phosphorylation and contribute to cytoskeleton tension, thus analysis of activity of ROCK is able to evaluate the range of intracellular tension[27, 44-47]. In our study, the ROCK activity was assayed through the testing of phosphorylation of its substrate, MYPT1[23, 28]. Results were in line with the cell morphology and cytoskeleton aforementioned. Moderate ROCK activity were found on NT and TPS contrast to the scarce expression on PT. Extremely higher ROCK activity could be observed on NTPS, nearly the summation of NT and TPS according to the semi-quantitative statistics. It was consistent with the cytoskeleton distribution analysis as aforementioned. Despite the excellent cell spreading on NT surface, small roughness meant cytoskeleton deformation in a single dimension , which meant relatively small cytoskeleton tension. Similarly, TPS provided rough macroporous surface but cells just took on elongated bodies rather than spread well on the rough surface, accompanied by less intracellular tension. As a matter of course, when good cell spreading met rough surface or marcopores, three-dimensional cytoskeleton distribution was formed and additional tension was produced. Besides, it is reported that substrate stiffness is also the factor that greatly influence intracellular tension in addition to cell spreading [28]**.** In our study, the fabricating of titanium coating and introduction of nanowires would probably decrease the elastic modulus and stiffness when considering the existence of macro and nano porous structures. It is demonstrated that the larger the elastic modulus, the higher the intracellular forces produced, and the greater the tendency towards osteogenesis[48, 49]. According to our study, NTPS with the lower elastic modulus had the relatively higher ability of osteogenesis, so it could be speculated that the influence brought by cell spreading may be far more than that from elastic modulus. Though, further study is necessary.

It has been considered that the cell fate concerning the osteogenic lineage is closely related to the cell spreading and cytoskeleton tension. Cells with well spreading and high skeleton tension undergo osteogenesis easily[23,50]. Our vitro experiment confirmed this version to some extent. Results showed that all the designed surface topographies, namely TPS, NT and NTPS, had comprehensive promotion on cell differentiation, as revealed by the enhanced ALP expression, obvious ECM mineralization and osteocalcin secretion, and remarkably increased gene expression contrast to the PT surface. Among these, the hierarchical NTPS structure possessed the better performance all the while. It could be preliminary deduced that cytoskeleton distribution on NT,TPS and NTPS, accompanied by corresponding cytoskeleton tension, had positive correlation with cell differentiation. In order to further confirm this relationship in our study, Y27632 was added in the medium to inhibit ROCK activity, leading to suppressed cytoskeleton tension. After Rock was inhibited, gene expression of Runx2, COL1 and OPN on different surfaces were drastically cut down to the same level for PT, NT and TPS. The gene expressions on NTPS were still a bit higher but the difference was greatly diminished. Hence, the correlation between cytoskeleton tension and cell differentiation has been convincingly verified. But detailed mechanism with respect to the ROCK and its downstream signaling pathway which act on cell differentiation still needs further study. The cytoskeletal tension are believed to influence cell differentiation through intracellular mechanotransduction[24, 51], which included the indirect one, namely signal pathways induced by focal adhesion formation and exposure of cryptic specific peptide sequences of kinase, and the direct one that is affected gene transcription by cytoskeleton reorganization and following deformation of cell nuclear skeleton[52-54]. According to the our study, the nanowire topography contribute to the cell spreading and the macroporous surface provide

three-dimensional deformation of cytoskeleton, so both well-developed focal adhesion and deformation of cell nuclear skeleton were involved, which probably means both indirect and direct mechanotransduction have made an effect together. Further research about the detailed mechanism are needed in the future. This study just confirmed the combination of nanowire and macropore topography brought about synergetic effect of cell cytoskeleton distribution on NTPS, which led to higher intracellular tension and better differentiation performance.

Conclusion

In this paper, NT, TPS and hierarchical NTPS surfaces were fabricated by plasma spraying and hydrothermal method. The NT structure led to better cell spreading, while TPS surface provided rough macroporous surface but poor cell spreading could be observed. When nanowire was introduced into TPS, better cell spreading and three-dimensional cytoskeleton deformation were obtained simultaneously, which led to higher intracellular tension. As a result, though NT and TPS surface both enhanced cell differentiation to some extent but NTPS had better performance. When cytoskeleton tension is inhibited, the difference diminished to a large extent. It points to that the NTPS hierarchical topography could influence cell morphology and cytoskeleton in a synergetic way and cause higher cytoskeleton tension, which was decisive for the better cell differentiation on NTPS surface.

Acknowledgements

This work is financially supported by the Opening Project of Shanghai Key Laboratory of Orthopaedic Implant (KFKT2014002).

References

1. A. Wisbey, P. J. Gregson, L. M. Peter and M. Tuke, *Biomaterials*, 1991, **12**, 470-473.
2. M. Long and H. J. Rack, *Biomaterials*, 1998, **19**, 1621-1639.
3. D. A. Puleo and A. Nanci, *Biomaterials*, 1999, **20**, 2311-2321.
4. J. Y. Rho, L. Kuhn-Spearing and P. Zioupos, *Medical engineering & physics*, 1998, **20**, 92-102.
5. A. Wennerberg and T. Albrektsson, *Clinical oral implants research*, 2009, **20**, 172-184.
6. A. G. Harvey, E. W. Hill and A. Bayat, *Expert review of medical devices*, 2013, **10**, 257-267.
7. M. Navarro, A. Michiardi, O. Castano and J. A. Planell, *Journal of the Royal Society Interface*, 2008, **5**, 1137-1158.
8. S. Bauer, P. Schmuki, K. von der Mark and J. Park, *Progress in Materials Science*, 2013, **58**, 261-326.
9. A. Palmquist, O. M. Omar, M. Esposito, J. Lausmaa and P. Thomsen, *Journal of the Royal Society Interface*, 2010, **7**, S515-S527.
10. X. Y. Liu, P. K. Chu and C. X. Ding, *Mat Sci Eng R*, 2010, **70**, 275-302.
11. H. M. Kim, T. Kokubo, S. Fujibayashi, S. Nishiguchi and T. Nakamura, *J Biomed Mater Res*, 2000, **52**, 553-557.
12. Y. K. Chen, X. B. Zheng, H. Ji and C. X. Ding, *Surf Coat Tech*, 2007, **202**, 494-498.
13. R. M. Pilliar, *J Biomed Mater Res-A*, 1987, **21**, 1-33.
14. L. Le Guehennec, A. Soueidan, P. Layrolle and Y. Amouriq, *Dental Materials*, 2007, **23**, 844-854.
15. W. C. Xue, X. Y. Liu, X. B. Zheng and C. X. Ding, *Biomaterials*, 2005, **26**, 3029-3037.
16. P. T. de Oliveira, S. F. Zalzal, M. M. Beloti, A. L. Rosa and A. Nanci, *Journal of Biomedical Materials Research Part A*, 2007, **80A**, 554-564.
17. E. K. F. Yim, E. M. Darling, K. Kulangara, F. Guilak and K. W. Leong, *Biomaterials*, 2010, **31**, 1299-1306.
18. W. J. Zhang, Z. H. Li, Q. F. Huang, L. Xu, J. H. Li, Y. Q. Jin, G. F. Wang, X. Y. Liu and X. Q. Jiang, *International journal of nanomedicine*, 2013, **8**, 257-265.
19. C. L. Zhao, P. Cao, W. P. Ji, P. Han, J. H. Zhang, F. Zhang, Y. Jiang and X. N. Zhang, *Journal of Biomedical Materials Research Part A*, 2011, **99A**, 666-675.
20. F. Wang, L. Shi, W. X. He, D. Han, Y. Yan, Z. Y. Niu and S. G. Shi, *Appl Surf Sci*, 2013, **265**, 480-488.
21. Y. T. Xie, X. B. Zheng, L. P. Huang and C. X. Ding, *Journal of Materials Science*, 2012, **47**, 1411-1417.
22. Y. T. Xie, H. Y. Ao, S. G. Xin, X. B. Zheng and C. X. Ding, *Mat Sci Eng C-Mater*, 2014, **38**, 272-277.
23. R. McBeath, D. M. Pirone, C. M. Nelson, K. Bhadriraju and C. S. Chen, *Dev Cell*, 2004, **6**, 483-495.
24. R. J. McMurray, M. J. Dalby and P. M. Tsimbouri, *J Tissue Eng Regen M*, 2015, **9**, 528-539.
25. B. K. K. Teo, S. T. Wong, C. K. Lim, T. Y. S. Kung, C. H. Yap, Y. Ramagopal, L. H. Romer and E. K. F. Yim, *Acs Nano*, 2013, **7**, 4785-4798.

26. B. K. K. Teo, S. Ankam, L. Y. Chan and E. K. F. Yim, *Method Cell Biol*, 2010, **98**, 241-294.
27. C. H. Seo, K. Furukawa, K. Montagne, H. Jeong and T. Ushida, *Biomaterials*, 2011, **32**, 9568-9575.
28. Y. R. V. Shih, K. F. Tseng, H. Y. Lai, C. H. Lin and O. K. Lee, *Journal of Bone and Mineral Research*, 2011, **26**, 730-738.
29. L. Xia, K. Lin, X. Jiang, B. Fang, Y. Xu, J. Liu, D. Zeng, M. Zhang, X. Zhang, J. Chang and Z. Zhang, *Biomaterials*, 2014, **35**, 8514-8527.
30. H. Ao, Y. Xie, H. Tan, X. Wu, G. Liu, A. Qin, X. Zheng and T. Tang, *Journal of Biomedical Materials Research Part A*, 2014, **102**, 204-214.
31. K. von der Mark, J. Park, S. Bauer and P. Schmuki, *Cell and tissue research*, 2010, **339**, 131-153.
32. F. Variola, J. B. Brunski, G. Orsini, P. T. de Oliveira, R. Wazen and A. Nanci, *Nanoscale*, 2011, **3**, 335-353.
33. A. Klymov, L. Prodanov, E. Lamers, J. A. Jansen and X. F. Walboomers, *Biomaterials Science*, 2013, **1**, 135-151.
34. C. Gonzalez-Garcia, S. R. Sousa, D. Moratal, P. Rico and M. Salmeron-Sanchez, *Colloid Surface B*, 2010, **77**, 181-190.
35. M. S. Lord, M. Foss and F. Besenbacher, *Nano Today*, 2010, **5**, 66-78.
36. C. H. Choi, S. H. Hagvall, B. M. Wu, J. C. Y. Dunn, R. E. Beygui and C. J. Kim, *Biomaterials*, 2007, **28**, 1672-1679.
37. B. Wang, Q. Cai, S. Zhang, X. P. Yang and X. L. Deng, *J Mech Behav Biomed*, 2011, **4**, 600-609.
38. M. J. Dalby, N. Gadegaard, M. O. Riehle, C. D. W. Wilkinson and A. S. G. Curtis, *Int J Biochem Cell B*, 2004, **36**, 2005-2015.
39. E. Lamers, X. F. Walboomers, M. Domanski, J. te Riet, F. C. M. J. M. van Delft, R. Luttge, L. A. J. A. Winnubst, H. J. G. E. Gardeniers and J. A. Jansen, *Biomaterials*, 2010, **31**, 3307-3316.
40. J. Y. Lim and H. J. Donahue, *Tissue engineering*, 2007, **13**, 1879-1891.
41. E. Martinez, E. Engel, J. A. Planell and J. Samitier, *Ann Anat*, 2009, **191**, 126-135.
42. M. Estevez, E. Martinez, S. J. Yarwood, M. J. Dalby and J. Samitier, *Journal of Biomedical Materials Research Part A*, 2015, **103**, 1659-1668.
43. L. Z. Zhao, S. L. Mei, P. K. Chu, Y. M. Zhang and Z. F. Wu, *Biomaterials*, 2010, **31**, 5072-5082.
44. T. Ozdemir, L. C. Xu, C. Siedlecki and J. L. Brown, *Integr Biol-Uk*, 2013, **5**, 1407-1416.
45. R. Guan, X. Xu, M. Chen, H. Hu, H. Ge, S. Wen, S. Zhou and R. Pi, *European journal of medicinal chemistry*, 2013, **70**, 613-622.
46. M. P. Walsh and W. C. Cole, *Journal of cerebral blood flow and metabolism : official journal of the International Society of Cerebral Blood Flow and Metabolism*, 2013, **33**, 1-12.
47. C. A. Hudson, K. J. Heesom and A. Lopez Bernal, *Molecular human reproduction*, 2012, **18**, 265-279.
48. A. J. Engler, S. Sen, H. L. Sweeney and D. E. Discher, *Cell*, 2006, **126**, 677-689.
49. S. J. Han, K. S. Bielawski, L. H. Ting, M. L. Rodriguez and N. J. Sniadecki, *Biophysical journal*, 2012, **103**, 640-648.
50. L. Z. Zhao, L. Liu, Z. F. Wu, Y. M. Zhang and P. K. Chu, *Biomaterials*, 2012, **33**, 2629-2641.

51. V. Vogel and M. Sheetz, *Nat Rev Mol Cell Bio*, 2006, **7**, 265-275.
52. L. A. Turner and M. J. Dalby, *Biomaterials Science*, 2014, **2**, 1574-1594.
53. M. J. Dalby, *Medical engineering & physics*, 2005, **27**, 730-742.
54. L. E. McNamara, R. Burchmore, M. O. Riehle, P. Herzyk, M. J. P. Biggs, C. D. W. Wilkinson, A. S. G. Curtis and M. J. Dalby, *Biomaterials*, 2012, **33**, 2835-2847.

Figures

Target gene	Direction	5'-3' Primer sequence
Runx2	F	5′-GCACCTACCAGCCTCACCATAC-3′
	R	5′-ACAGCGACTTCATTCGACTTCC-3′
COL1	F	5′-CATGAGCCGAAGCTAACCC-3′
	R	5′-TGTGGCAGATACAGATCAAGCA-3′
OPN	F	5′-CTTTCACTCCAATCGTCCCTAC-3′
	R	5′-CCTTAGACTCACCGCTCTTCAT-3′
β-actin	F	5′-CCAGCCTTCCTTCTTGGGTAT-3′
	R	5′-TGTTGGCATAGAGGTCTTTACGG-3′

Table. 1. Primers for real-time polymerase chain reaction (PCR). F, forward; R, reverse; Runx2, runt-related transcription factor 2; COL1, collagen type I; OPN, osteopontin.

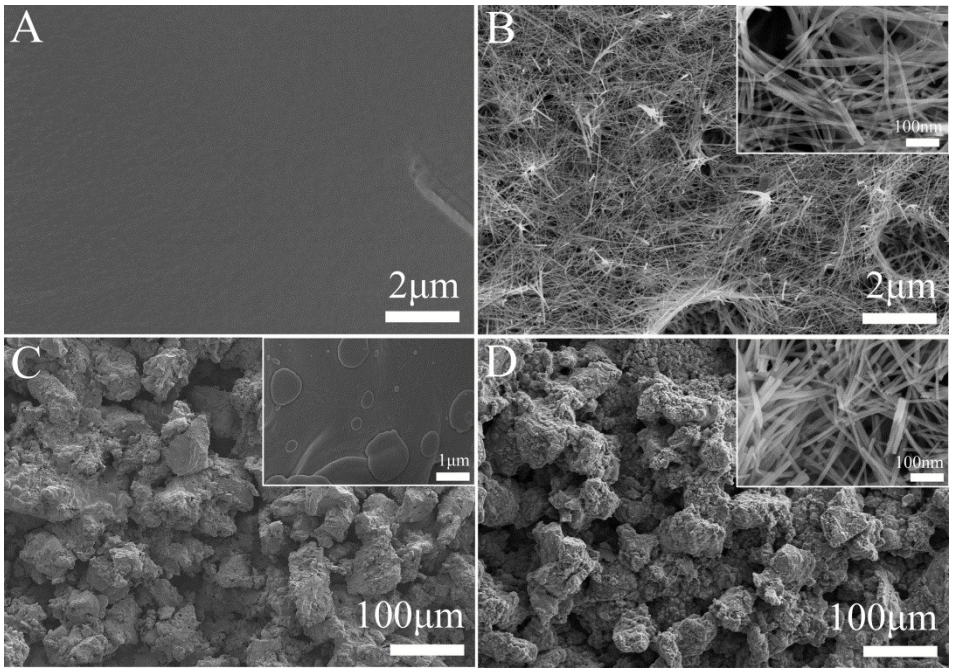

Fig. 1. SEM images of the fabricated surface topography at low and high magnification. (A) PT; (B) NT; (C) TPS; (D) NTPS. Anisotropic nanowires was observed on NT. Diameters of nanowires were about 20-50 nm as showed in the inserted picture. No obvious differences were found in the low magnification views of TPS and NTPS. In the high magnification, the particle surface was relatively smooth on TPS while nanowire was observed for NTPS.

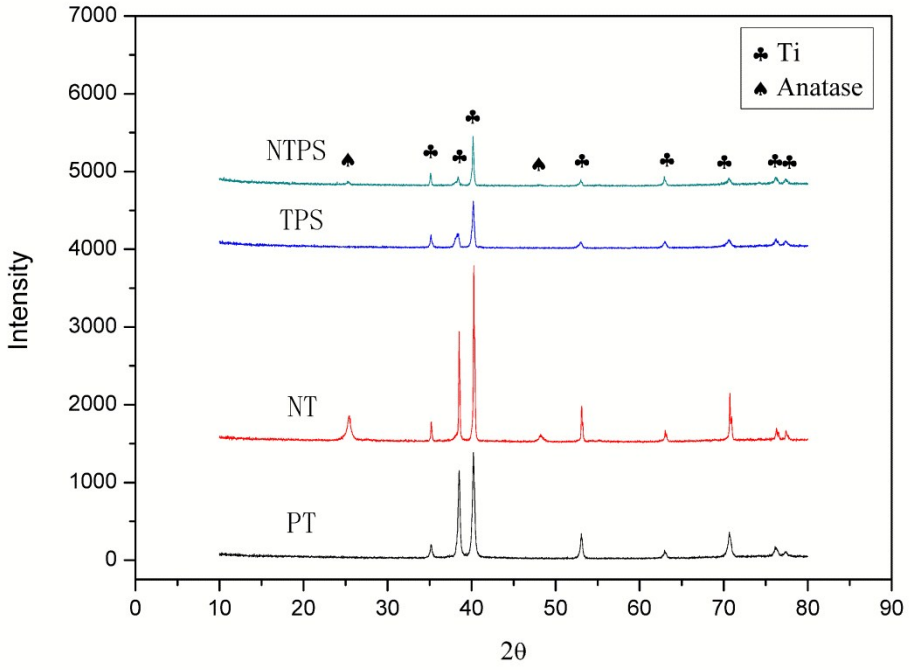

Fig. 2. XRD patterns of different samples. Phase of anatase was observed on the surface of NT and NTPS.

Surface topography	Ra / μm
PT	0.88 ± 0.05
NT	1.58 ± 0.09
TPS	15.05 ± 1.29
NTPS	16.45 ± 2.00

Table. 2. Roughness of four fabricated surfaces. TPS and NTPS had approximate roughness around 15μm while nanowire make little effect on roughness

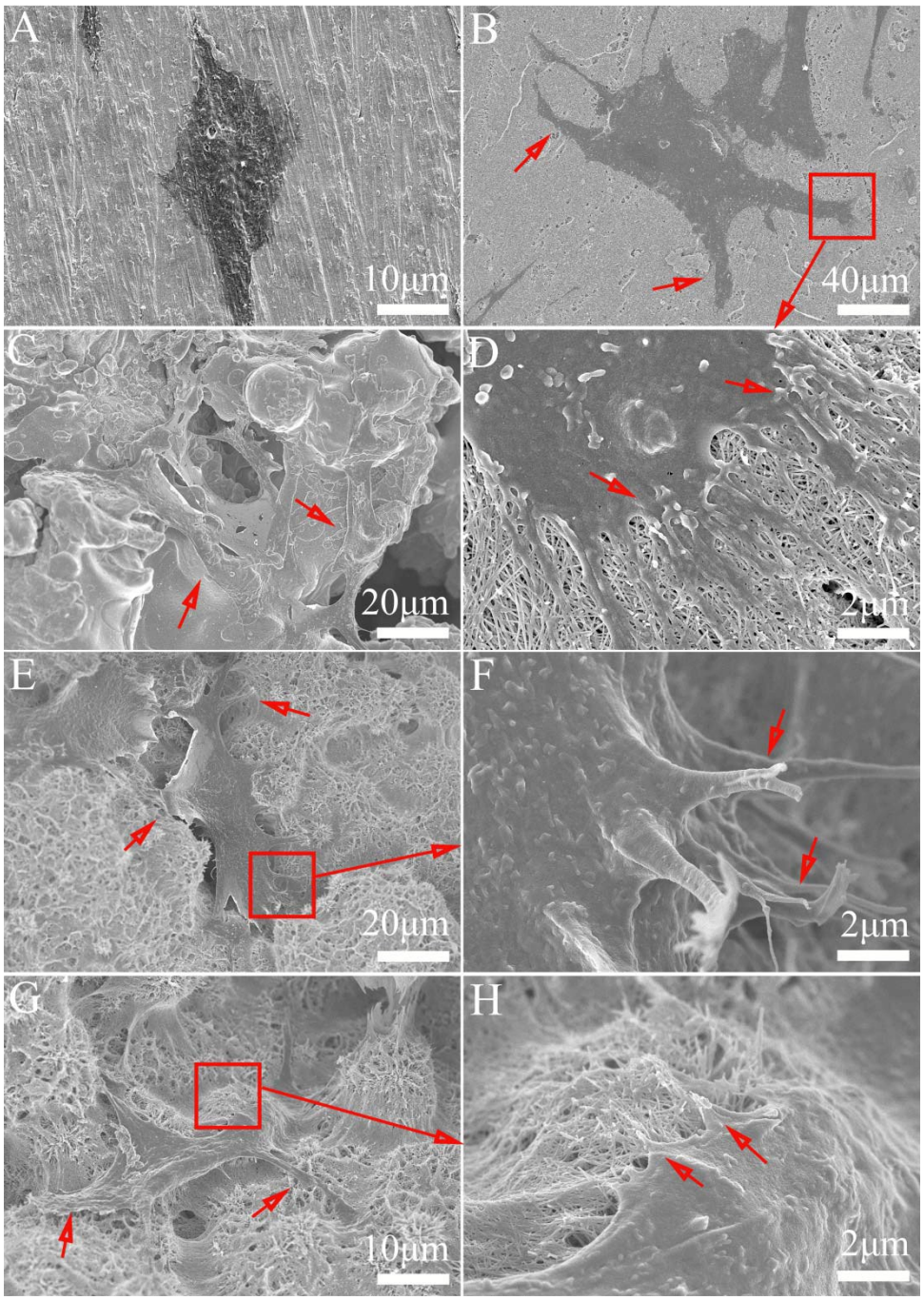

Fig. 3. SEM pictures showing the morphology of cells after 1d of culture on different samples. Arrows showed typical characteristics of cells. (A) PT; cell presented spindle morphology with less-stretched body (B) NT; cell was observed with well-stretched cytoskeleton (C) TPS; cell showed extend bodies adapted to the rough surface with insufficient spread and little filopodia; (D) magnification picture of B; arrows points to obvious long filopodia on the edge of cell; (E, G) NTPS; fully-spread cell and 3-D distributive cytoskeleton were observed (F, H) magnification picture of E, G; abundant filopodia could be seen at the periphery of cytoskeleton.

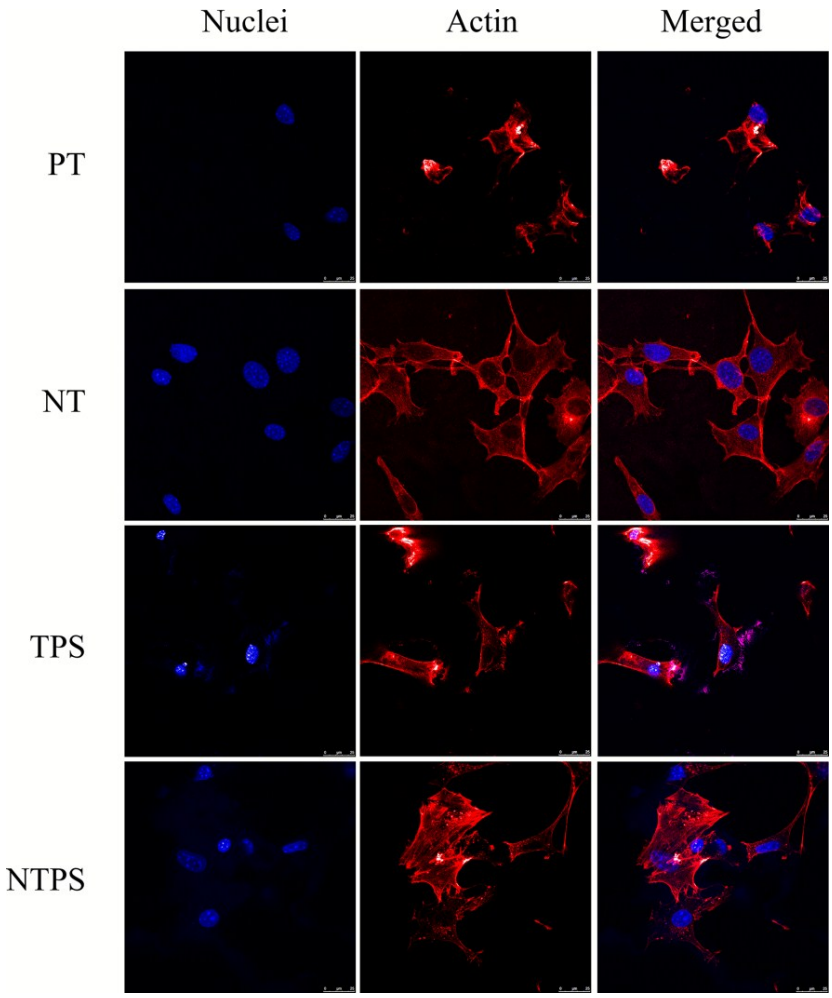

Fig. 4. Fluorescence staining pictures of MC3T3 cells after seeded by 1day on different surfaces. Red, actin cytoskeleton stained with TRITC-phalloidin; blue, nuclei stained with DAPI. "Merged" represent the merged images of nuclei and actin cytoskeleton. Cytoskeleton distribution in fluorescence staining pictures were in accord with the SEM pictures.

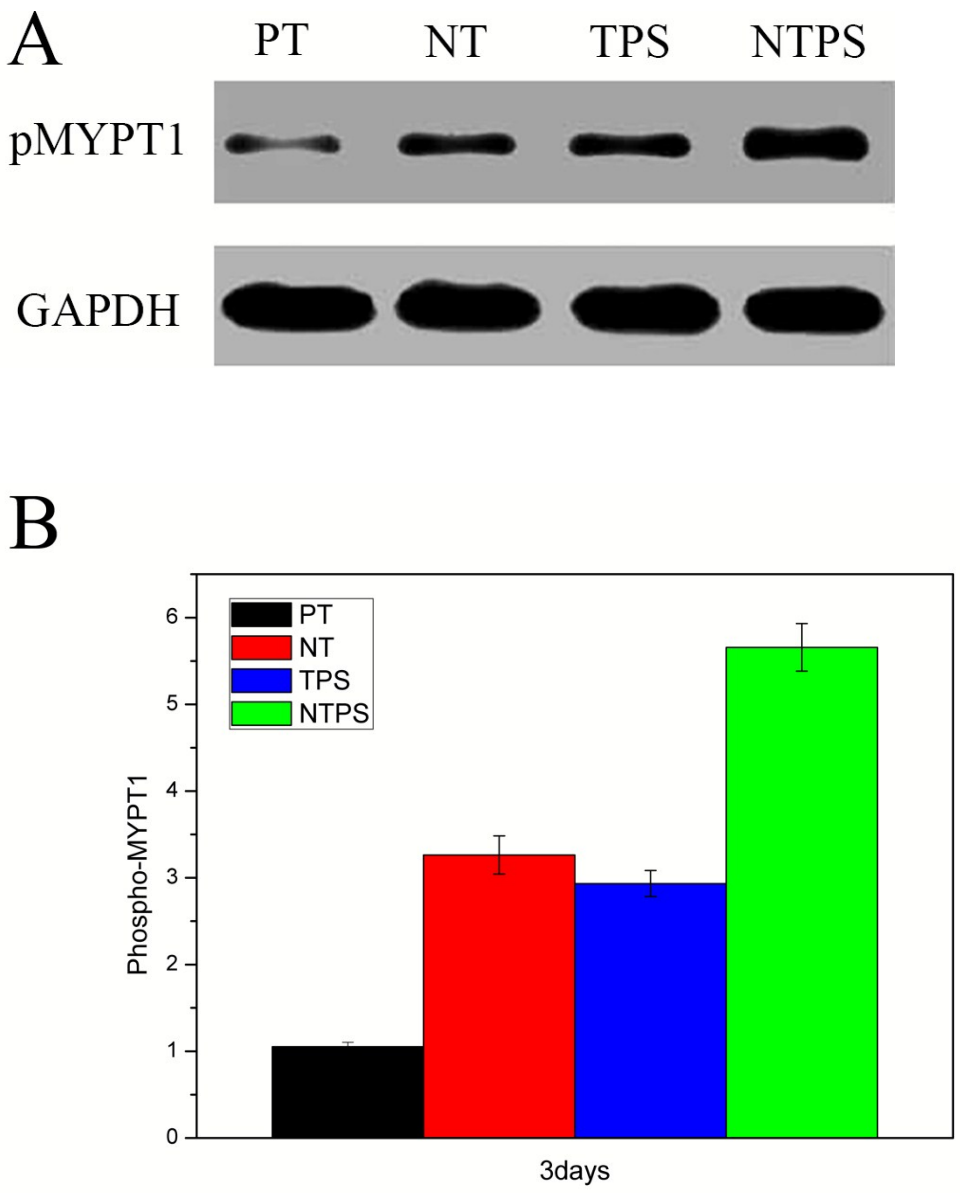

Fig. 5. (A) Western blotting of pMYPT1 after 3 days' culture. (B) Semi-quantitative analysis of the western blotting result.

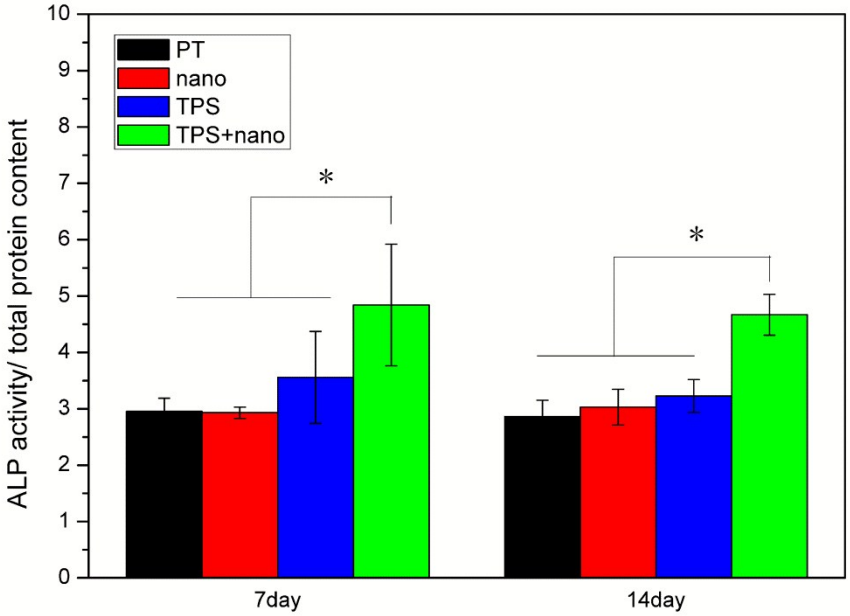

Fig. 6. ALP activity on different samples cultured for 7d and 14d. Values are normalized to the total protein content. * represents $p < 0.05$.

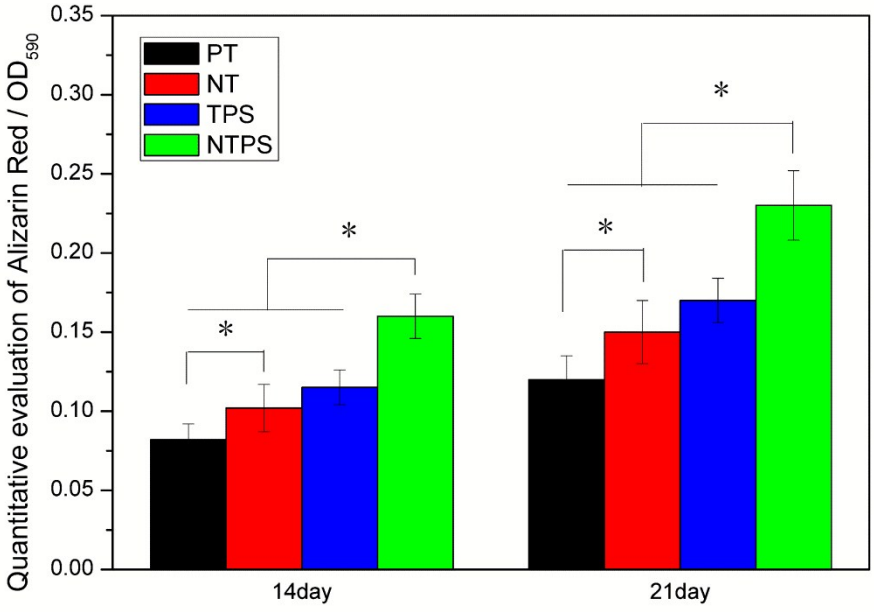

Fig. 7. Calcium deposition essay by quantitative analysis of Alizarin Red staining after 14 and 21 days, * represents $p < 0.05$.

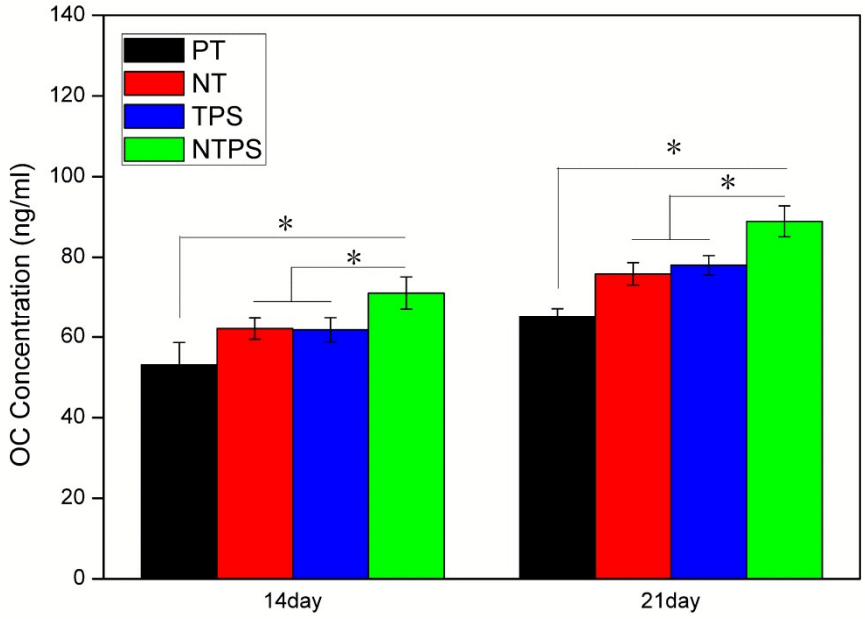

Fig. 8. Quantitative analysis of osteocalcin secretion by ELISA after 14 and 21 days. * represents $p < 0.05$.

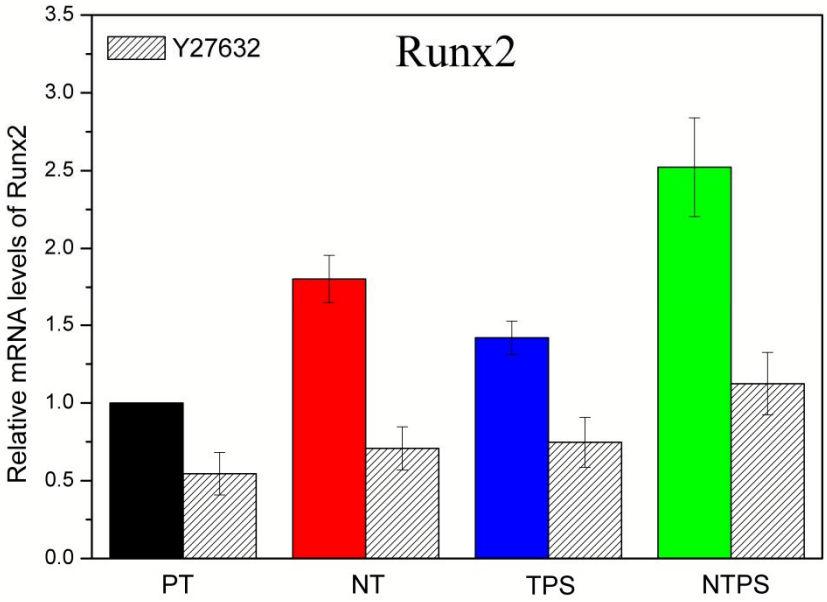

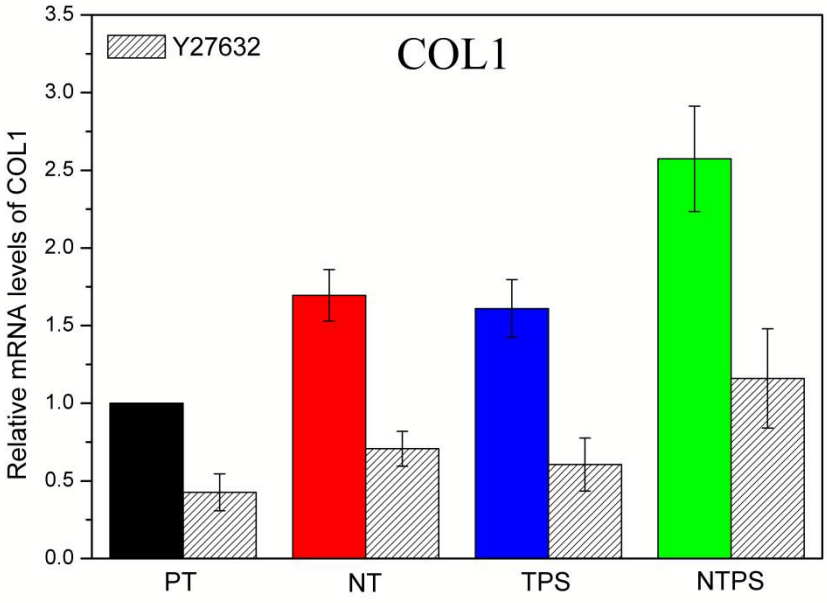

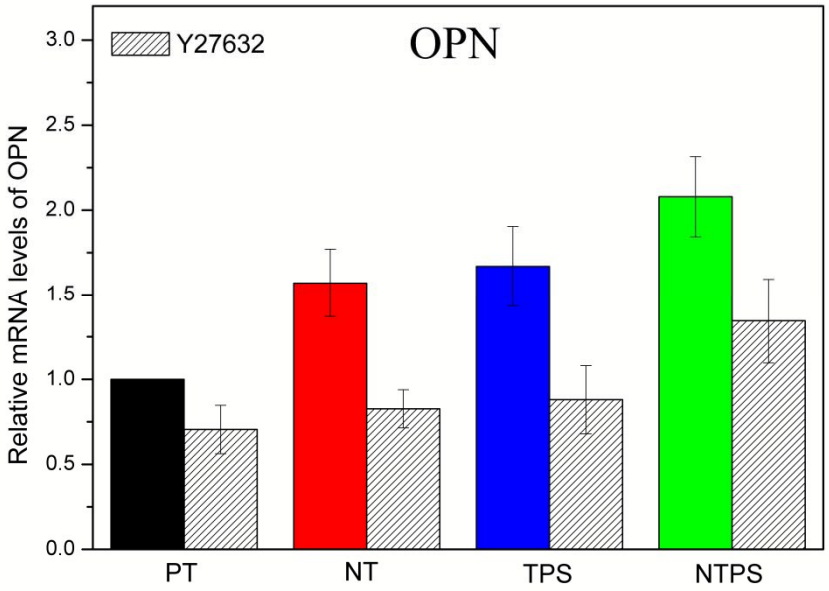

Fig. 9. Relative expressions of Runx2, COL1 and OPN after cultured on different substrates for 14 days, all values normalized to GAPDH and presented relative to the results of PT. Y27632 was added for each sample at the concentration of 10μM for comparison.

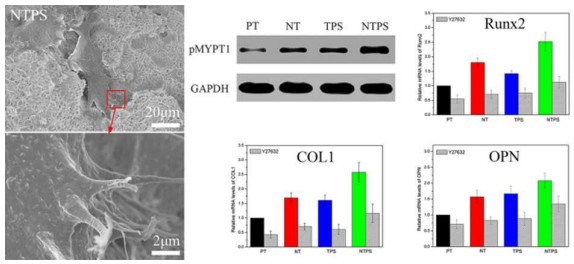

Synergistic effect of cytoskeleton distribution on macro/nano surface led to higher intracellular tension and better differentiation performance.